Mathematical and Computer Modelling 55 (2012) 1770–1781

Contents lists available at SciVerse ScienceDirect

Mathematical and Computer Modelling

journal homepage: www.elsevier.com/locate/mcm

Shape reconstruction of cardiac ischemia from non-contact intracardiac recordings: A model study

Diego Álvarez [a,*], Felipe Alonso-Atienza [b], José Luis Rojo-Álvarez [b], Arcadi García-Alberola [c], Miguel Moscoso [a]

[a] Instituto Gregorio Millán, Universidad Carlos III de Madrid, 28911 Leganés, Madrid, Spain

[b] Departamento de Teoría de la Señal y Comunicaciones, Universidad Rey Juan Carlos, Camino del Molino s/n, 28943 Fuenlabrada, Madrid, Spain

[c] Servicio de Cardiología, Hospital Universitario Virgen de la Arrixaca, Carretera Madrid-Cartagena s/n, 30120 El Palmar, Murcia, Spain

ARTICLE INFO

Article history:
Received 13 May 2011
Received in revised form 29 September 2011
Accepted 1 November 2011

Keywords:
Ischemia
Non-contact mapping
Inverse problem
Level set

ABSTRACT

We present a new approach for the reconstruction of ischemic regions from only a few non-contact intracardiac recordings. Hence, it is desirable to exploit the spatio-temporal correlations contained in the data. To this end, we incorporate a time-dependent monodomain model of the cardiac electric activity into the inversion scheme. In order to take into account the electrophysiological alterations of ischemic regions, we also introduce appropriate variations of the model parameters. This approach allows us to perform the reconstruction of the affected regions successfully using only a few recording sites. The reconstruction process is based on level set techniques. Our numerical experiments in a bi-dimensional model of cardiac tissue validate our approach.

1. Introduction

Mathematical modeling plays an important role in the research of the electrophysiological behavior of the human heart [1–3]. For example, it is essential in the development of procedures to reconstruct its electrical activity from voltage measurements, i.e., to solve the, so called, inverse problem of electrocardiography (IPE) [4,5]. An accurate solution to the IPE can provide important information for the diagnosis of cardiac electrical conduction defects and other cardiac related health issues, such as ischemic heart disease, produced by the lack of blood supplied by the coronary arteries to the heart muscle.

We can distinguish different scenarios in IPE depending on where the electrodes are placed. In a daily routine, clinicians use body surface electrocardiograms (ECGs) to diagnose the health of a patient's heart. Also, they can use non-contact electrodes inside a heart cavity to register intracardiac electrograms (EGMs) [6,7]. In this paper, we will consider the latter case. We seek to retrieve some model parameters from EGMs. These parameters will give us information about tissue regions affected by ischemia.

From a mathematical point of view, the IPE is ill-posed due, in part, to smoothing and attenuation of the cardiac signal during its propagation in the medium between the heart muscle and the electrodes [8,5]. To mitigate these difficulties, an extensive number of regularization techniques have been proposed in the literature, mostly of the Tikhonov–Philips type [4,9,10]. However, in these works each time instant is treated independently from the others, thus ignoring the spatio-temporal correlation information contained in the measurements. To overcome this problem, several spatio-temporal regularization methods have been proposed including the Twomey technique [11], simultaneous regularization over all

* Correspondence to: E.P.S. Universidad Carlos III de Madrid, Leganés, 28911 Madrid, Spain. Tel.: +34 916248824; fax: +34 916249129.
E-mail address: jdiego@math.uc3m.es (D. Álvarez).

0895-7177/$ – see front matter © 2011 Elsevier Ltd. All rights reserved.
doi:10.1016/j.mcm.2011.11.025

considered time instants [12], simultaneous imposition of spatial and temporal constraints [13], and Kalman filtering [14]. Some of these techniques have been complemented with model-based approaches imposing a parameterized function to the solution [15–19]. The IPE has also been analyzed in terms of statistical criteria [20,21]. More recently, Ghost et al. have explored the performance of Tikhonov–Philips regularization tools using the one-norm constraint [22].

In this paper, we follow a different approach. We combine a bi-dimensional model of cardiac propagation and a model of electrode recording inside the heart. The knowledge of the cardiac excitation process, given by the cardiac propagation model, is introduced in the inverse problem formulation allowing us to exploit the spatio-temporal correlation contained in the EGMs. Hence, only a few electrodes are needed to reconstruct the regions of interest successfully. To incorporate an ischemia, we allow two parameters of the bioelectrical model to have different values inside and outside the damaged tissue. Several numerical experiments validate our approach.

To solve the IPE, we propose a shape-based approach and we apply level-set techniques. Level-set techniques were originally introduced for computational front propagation in [23], and for solving inverse problems in [24]. Since then, they have been widely used for solving inverse problems in different applications with great success [25–27] (see [28] for a recent overview). Also, a level-set formulation has been proposed in [29] to identify ischemic regions from body surface measurements. They use a stationary model to represent the resting potentials on the heart.

The paper is organized as follows. In Section 2, we present the mathematical model used for describing the cardiac electrical activity and the associated intracardiac recordings. In Section 3, we formulate our approach for the reconstruction of the ischemic regions, and we detail the inversion algorithm. Section 4 contains the numerical experiments using synthetic data. Finally, the conclusions are summarized in Section 5.

2. Mathematical model

In this section, we present the mathematical model relating the cardiac sources to intracardiac measurements which accounts for descriptions of single cell dynamics, bioelectric propagation, ischemic conditions and intracardiac potentials.

2.1. Bioelectric cardiac source model

Cardiac cell dynamics are modeled here according to the two-current ionic model defined by Mitchell and Schaeffer [30]. This phenomenological model only incorporates an inward current (representing sodium and calcium currents) and an outward current (representing potassium current). Despite its simplicity, the two-current model is able to closely reproduce the restitution properties of the cardiac tissue and to simulate other complex electrophysiological behaviors such as spatial variations of the action potential duration (APD) [31]. It has also provided important insights into key arrhythmogenic factors, like alternans and discordant alternans [30,32,33]. The formulation of this model consists of two differential equations for two variables: the transmembrane voltage $v(t)$ and the inactivation gate variable $h(t)$, both of which are dimensionless and scaled to vary between 0 and 1. The temporal variation of the transmembrane voltage[1] $v(t)$ is described by the differential equation

$$\frac{dv}{dt} = F(v, h) = J_{in}(v, h) + J_{out}(v) + J_{stim}(t). \tag{1}$$

where J_{in} and J_{out} represent the inward and outward currents, respectively, and they are given by

$$J_{in}(v, h) = \frac{h(1 - v)v^2}{\tau_{in}} \quad \text{and} \tag{2}$$

$$J_{out}(v) = -\frac{v}{\tau_{out}}, \tag{3}$$

and J_{stim} denotes the external stimulus current. The inward current J_{in} is regulated by the inactivation gating variable $h(t)$ obeying the equation

$$\frac{dh}{dt} = \begin{cases} \dfrac{1 - h}{\tau_{open}}, & v < v_{crit} \\ \dfrac{-h}{\tau_{close}}, & v > v_{crit}. \end{cases} \tag{4}$$

The two-current model contains five parameters: τ_{in}, τ_{close}, τ_{out}, τ_{open}, and v_{crit} (see Table 1). The first four parameters are time constants. They characterize the four phases of the cardiac action potential (AP): τ_{in} specifies the strength of the inward current and represents the upstroke of the AP; τ_{close} is the time interval over which h closes and corresponds to the plateau phase of the AP; τ_{out} controls the strength of the outward current and determines the decay phase of the AP; finally, the gate h reopens with time constant τ_{open} (which is equivalent to the recovery phase of the AP). The last parameter, v_{crit}, is the change-over voltage.

[1] Using a simple transformation, v can be scaled back to appropriate physiological values.

Table 1
Parameter values for the two-current model, obtained from [31].

Parameter	Value (units)
τ_{in}	0.2 ms
τ_{out}	10 ms
τ_{open}	130 ms
τ_{close}	150 ms
v_{crit}	0.13

2.2. Cardiac bioelectric propagation model

Cardiac bioelectric propagation is simulated following the so-called monodomain formalism by inserting a diffusive term in (1) [34]. Hence, the transmembrane voltage $v(\mathbf{r}, t)$ inside the cardiac tissue Ω is governed by the reaction–diffusion partial differential equation

$$\frac{\partial v}{\partial t} = \kappa \nabla^2 v + F(v, h), \tag{5}$$

where the conductivity of the cardiac tissue is set to $\kappa = 10^{-3}$ cm^2/ms [31]. According to the monodomain formalism, the diffusive term corresponds to the transmembrane current $i_m = \kappa \nabla^2 v$, which represents the current flow through the cardiac cell membrane during the activation and repolarization processes. Eqs. (4) and (5) are supplemented using initial conditions

$$v(\mathbf{r}, 0) = v_{rest}, \qquad h(\mathbf{r}, 0) = 1, \quad \text{in } \Omega, \tag{6}$$

for v and h, respectively, as well as no-flux boundary conditions

$$\frac{\partial v}{\partial \mathbf{n}} = 0 \quad \text{on } \partial\Omega, \tag{7}$$

where $\partial\Omega$ denotes the boundary of the cardiac tissue and v_{rest} is the resting potential. Eqs. (1)–(7) define our cardiac bioelectric propagation model. We have considered the cardiac tissue having a two-dimensional geometry. An advantage of this model is that analytical results that characterize the AP and its propagation throughout the cardiac tissue can be extracted. In particular, the first APD and the conduction velocity (CV) of the AP are given by Cain and Schaeffer [31]

$$APD = \tau_{close} \ln\left(\frac{\tau_{out}}{4\tau_{in}}\right), \tag{8}$$

$$CV = \frac{1}{4}\left(3 \cdot \sqrt{1 - \frac{4\tau_{in}}{\tau_{out}}} - 1\right)\sqrt{\frac{2\kappa}{\tau_{in}}}. \tag{9}$$

For the set of parameters presented in Table 1, the two-current model predicts an APD of 379 ms and a CV of 46.9 cm/s. These values are within the range of those corresponding to the healthy tissue.

2.3. Model of ischemia

Acute ischemia elicits profound electrophysiological alterations in cardiac cells which are mainly caused by hypoxia, hyperkalemia and acidosis [35–37]. Hypoxia is a pathological condition in which an adequate oxygen supply is deprived. This causes a significant reduction of the APD in the cardiac myocytes. Hyperkalemia refers to the elevation of extracellular potassium concentration which decreases excitability and delays recovery of excitability of the cardiac tissue. Major electrophysiological consequences of hyperkalemia include increase of the resting potential, and the reduction of (i) the AP upstroke, (ii) the AP amplitude and (iii) the CV. Finally, acidosis is produced by a reduction in pH which decreases the maximum conductance of sodium and calcium currents. Effects of acidosis manifest as a reduction in the amplitude of the AP and a slight increase of the resting potential. A number of mathematical models have been used to analyze the electrophysiological effects of myocardial ischemia on cell [37] and tissue levels [38–40]. Compared to normal conditions, these studies show that, after approximately 10 min from the onset of the ischemia, the resting potential increases by 10%, the APD decreases by 64%, and the amplitude of the AP decreases by 30%. In addition, the conduction velocity (CV) also experiences a reduction of 68%. In this paper, we model acute ischemic conditions by appropriately modifying τ_{in}, and by introducing v_{rest} in (2) and (3), so that

$$J_{in}(v, h) = \frac{h(1 - v)(v - v_{rest})^2}{\tau_{in}}, \quad \text{and} \tag{10}$$

$$J_{out}(v) = -\frac{v - v_{rest}}{\tau_{out}}. \tag{11}$$

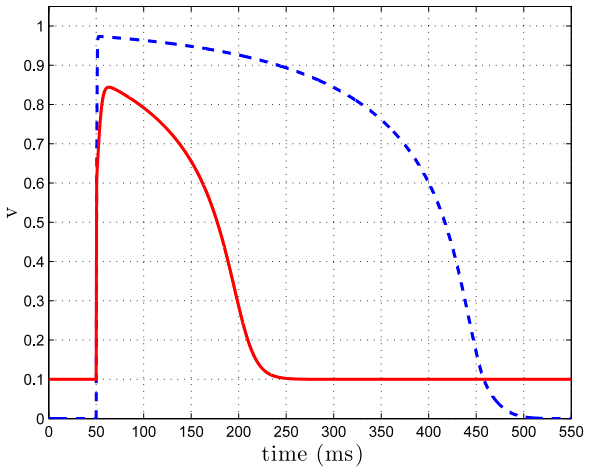

Fig. 1. Resulting AP from the two-current model under normal (dashed line) and ischemic conditions (solid line).

Note that in these equations $\tau_{in} = \tau_{in}(\mathbf{r})$ and $v_{rest} = v_{rest}(\mathbf{r})$. These parameters characterize the ischemic region, while the rest of the parameters in the model remain constant. Increasing the value of τ_{in} from 0.2 to 1.0 ms in the ischemic cells decreases the APD to 137 ms according to (8), and CV from 46.9 to 14.8 cm/s according to (9). On the other hand, setting $v_{rest} = 0.1$ for the ischemic cells increases a 10% the resting potential mainly due to hyperkalemia and, to less extent, due to acidosis [37]. Fig. 1 shows the resulting AP for both healthy (dashed line) and ischemic cells (solid line). Effects of ischemia on the CV can be appreciated in Fig. 3(a). Setting $\tau_{in} = 1.0$ ms and $v_{rest} = 0.1$ allows us to describe the main electrophysiological changes on cell and tissue levels corresponding to altered ischemic conditions. In spite of the simplicity of this model, the induced effects of ischemia are in agreement with previous computer models [37–40]. At the tissue level, we use a regional model of ischemia where the parameters $\tau_{in}(\mathbf{r})$ and $v_{rest}(\mathbf{r})$ vary linearly between the healthy and the acute ischemic regions. Fig. 2 represents an example of the spatial variation of τ_{in} in our model of cardiac tissue. In this figure, there is a circular-shaped ischemic zone S such that

$$\tau_{in}(\mathbf{r}) = \begin{cases} 0.2 \text{ ms} \leq \tau_{in} \leq 1.0 \text{ ms} & \text{inside } S, \\ 0.2 \text{ ms} & \text{outside } S. \end{cases} \tag{12}$$

Likewise,

$$v_{rest}(\mathbf{r}) = \begin{cases} 0 \leq v_{rest} \leq 0.1 & \text{inside } S, \\ 0 & \text{outside } S. \end{cases} \tag{13}$$

The rest of the parameters remain constant within the whole tissue.

2.4. Model of intracardiac recordings

Motivated by the current non-contact endocardial mapping systems used in electrophysiology studies [6,7], we consider monopolar intracavitary probe electrodes. According to the volume conductor theory [41], the electric potential registered at a point $\mathbf{r}_i$ within a cardiac chamber is given by

$$\phi_i(t) = \frac{1}{4\pi\sigma} \int_{\Omega} \frac{i_m(\mathbf{r}, t)}{|\mathbf{r} - \mathbf{r}_i|} d\mathbf{r}, \tag{14}$$

where σ denotes the conductivity of the blood. This last expression relates the cardiac sources $i_m(\mathbf{r}, t)$ to non-contact measurements $\phi_i(t)$. Therefore, using (14) together with the model of cardiac excitation and propagation given by (1), (10), (11), (4) and (5) subject to (6) and (7) comprise a complete description of our direct problem. The properties of the cardiac tissue are given by $\tau_{in} = \tau_{in}(\mathbf{r})$ and $v_{rest} = v_{rest}(\mathbf{r})$, and by the space independent parameters τ_{close}, τ_{out}, τ_{open}, and v_{crit}. Fig. 3 represents the numerical experiment setup used in this study. In this case, a rectangular piece of the cardiac tissue containing an ischemic region at the center has been considered. As a result, the cardiac electric impulse propagates slowly at the ischemic region. The time dependent intracavitary recording shown in panels (b) and (c) are measured at point labeled as (1) above the cardiac tissue. Panel (b) represents the registered recording when no ischemic zone is considered, while the measurement shown in panel (b) is obtained when a central ischemic region is present. An elevation of the repolarization wave can be observed due to ischemia [42].

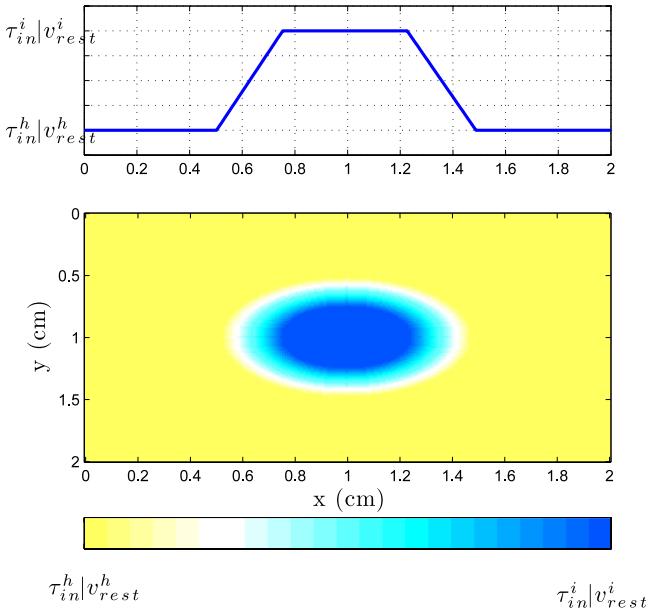

Fig. 2. Regional model of ischemia. Parameters τ_{in} and v_{rest} vary linearly between values $\tau^h_{in} = 0.2$ ms and $v^h_{rest} = 0$ for the healthy tissue, respectively; and $\tau^i_{in} = 1.0$ ms and $v^i_{rest} = 0.1$ for the ischemic tissue, respectively.

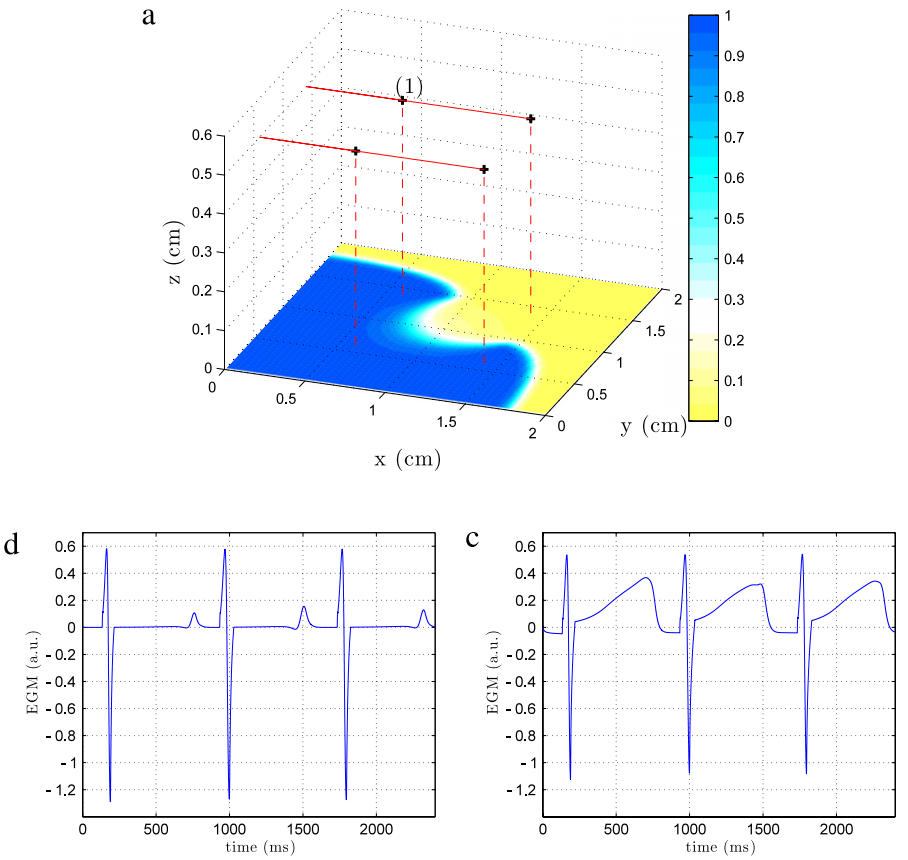

Fig. 3. Numerical experiment setup. (a) Snapshot of the electrical propagation of the cardiac impulse over a bi-dimensional tissue having a central ischemic zone. The electrical activity is registered by non-contact electrodes placed at different locations. Examples of non-contact intracardiac recordings (in arbitrary units a.u.) at location labeled as (1) when (b) no ischemia is present and (c) a central ischemic zone is considered.

3. Shape reconstruction of ischemia

Let $\tilde{\phi}_i$ be the true measurements and ϕ_i be the simulated data. Using this notation, $\tilde{i}_m(\mathbf{r}, t)$ solves the direct problem with the correct parameters $\tilde{\tau}_{in}(\mathbf{r})$ and $\tilde{v}_{rest}(\mathbf{r})$. Hence, the objective of our inverse formulation is to reconstruct the unknown parameter distributions $\tilde{\tau}_{in}(\mathbf{r})$ and $\tilde{v}_{rest}(\mathbf{r})$ in the cardiac tissue from the measured data. To this end, our direct model potentials ϕ_i are compared to the measured intracavitary potentials $\tilde{\phi}_i$, so the model parameters are iteratively updated to minimize the mismatch between calculated and measured data. This can be expressed in terms of the minimization of the least-squares cost functional

$$\mathcal{J}(\tau_{in}, v_{rest}) = \frac{1}{2} \|\mathcal{R}(\tau_{in}, v_{rest})\|_2^2, \tag{15}$$

where

$$\mathcal{R}(\tau_{in}, v_{rest}) = \phi(\tau_{in}, v_{rest}) - \tilde{\phi} \tag{16}$$

being ϕ and $\tilde{\phi}$ the matrix containing all simulated and measured intracavitary potentials, respectively. Eq. (16) describes the mismatch between these physically measured data and the data corresponding to a guess (τ_{in}, v_{rest}). Instead of solving the inverse problem for the entire functions $\tilde{\tau}_{in}(\mathbf{r})$ and $\tilde{v}_{rest}(\mathbf{r})$, we solve the shape reconstruction problem that only requires to find the shape S of the ischemia. Our shape-based approach is motivated by the fact that we only use a few intracavitary electrodes. Hence, the amount of data is very limited, giving rise to low resolution images when standard pixel-based techniques for the inversion are used. Under these circumstances, compared to standard pixel-based techniques for inversion, shape reconstruction approaches reduce the dimensionality of the inverse problem, preserve the sharp edges, and enhance the contrast in the images (see, for example, [26] for a more detailed discussion). In our shape inversion, the unknown shape S of the ischemic region is implicitly represented by a smooth level-set function ψ that is negative inside the ischemic region and positive outside it. Hence, the unknown parameter distributions can be described by

$$\tau_{in}(\mathbf{r}) = \begin{cases} 1.0 \text{ ms} & \text{inside } S, \quad \text{where } \psi(\mathbf{r}) \leq 0, \\ 0.2 \text{ ms} & \text{outside } S, \quad \text{where } \psi(\mathbf{r}) > 0, \end{cases} \tag{17}$$

and

$$v_{rest}(\mathbf{r}) = \begin{cases} 0 & \text{inside } S, \quad \text{where } \psi(\mathbf{r}) \leq 0, \\ 0.1 & \text{outside } S, \quad \text{where } \psi(\mathbf{r}) > 0. \end{cases} \tag{18}$$

In these equations, the parameters $\tau_{in}(\mathbf{r})$ and $v_{rest}(\mathbf{r})$ define the ischemic region. Since both parameters define the same shape S, we will use only τ_{in} to define S from now on. Note that the boundary δS of the ischemia consists of all points such that $\psi(\mathbf{r}) = 0$. We will indicate the dependence of τ_{in} on the level-set function ψ, by $\tau_{in}(\psi)$. The main advantage of this implicit representation of the unknown shape by a level-set function is its capability of automatically splitting and merging shapes during the reconstruction. We note that the value of τ_{in} inside the ischemic region is assumed to be constant (and known) during the reconstruction. Therefore, modeling error is introduced by incomplete knowledge of the parameter distribution inside the ischemia. Indeed, the piecewise distribution assumed in (17) does not correspond to the true one defined in (12). The value of τ_{in} in (12) increases linearly from the boundary of the ischemia up to a certain point inside S. With the above definitions, we can formulate the shape reconstruction problem using level set as follows. Find a level set function ψ that minimizes the shape least squares cost functional

$$\mathcal{J}(\psi) = \frac{1}{2} \|\mathcal{R}(\psi)\|_2^2, \tag{19}$$

where we denote $\mathcal{R}(\psi) = \mathcal{R}(\tau_{in}(\psi))$. The objective is to find a level set function $\hat{\psi}$ such that using $\tau_{in}(\hat{\psi})$ (and $v_{rest}(\hat{\psi})$) in (4) and (5) (with (10) and (11)) the computed data match the measured data. To solve the shape reconstruction problem, we follow a time evolution approach [27,43]. We introduce an artificial time ξ, related to the iterative step of the reconstruction process, and use the evolution law

$$\frac{d\psi}{d\xi} = f(\mathbf{r}; \xi) \tag{20}$$

for the unknown level set function ψ. The purpose of the evolution law (20) is to reduce, and eventually minimize (19). In this formulation, the least-squares cost functional (19) depends on the artificial time ξ. Hence, we can evaluate its derivative with respect to the time ξ applying the chain rule

$$\begin{aligned} \frac{d\mathcal{J}}{d\xi} &= \frac{\partial \mathcal{J}}{\partial \tau_{in}} \frac{\partial \tau_{in}}{\partial \psi} \frac{d\psi}{d\xi} \\ &= \left\langle \mathbf{grad}_{\tau_{in}} \mathcal{J}(\mathbf{r}; \xi), \frac{\partial \tau_{in}}{\partial \psi} \frac{d\psi}{d\xi} \right\rangle_P \\ &= \int_\Omega d\mathbf{r}\, \mathbf{grad}_{\tau_{in}} \mathcal{J}(\mathbf{r}; \xi) \tau_{in} \delta(\psi) f(\mathbf{r}; \xi), \end{aligned} \tag{21}$$

Algorithm 1 : *Shape reconstruction of ischemia*

1. Set $n = 0$ and start introducing a level set function $\psi^{(0)}(\mathbf{r})$. The result is a piecewise distribution, as shown in Fig. 4 (b).
2. Apply J_{stim}, and solve the direct problem using the latest guess $\tau_{in}(\psi^{(n)})$. This gives rise to the predicted data $\phi_j^{(n)}$.
3. Compute the residuals $\mathcal{R}_j = \phi_j^{(n)} - \tilde{\phi}_j$, and solve the adjoint problem (24)–(26). The gradient direction of $\mathcal{J}(\psi^{(n)})$ is given by (23).
4. Compute $f^{(n)}(\mathbf{r})$ given by (22), and apply the update (27) to the level set function $\psi^{(n)}$. Smooth $f^{(n)}(\mathbf{r})$ by solving a heat equation. It is well known that the gradient directions computed directly from the adjoint formulation lead to rapidly varying functions in a spatial fine-scale, giving rise to $f^{(n)}(\mathbf{r})$ that exhibit strong variations. This introduces instabilities during the reconstruction process that are necessary to avoid (see [28] for details).
5. Check the stopping criterion. In our case we have chosen as stopping criteria that the cost becomes stationary. If this is not satisfied, go to step 2) with $n = n + 1$.

where $\langle , \rangle_P$ represents the canonical inner product in the parameter space P. Using this equation, we can select a descent direction for the cost functional by choosing

$$f(\mathbf{r}; \xi) = -\mathbf{grad}_{\tau_{in}} \mathcal{J}(\mathbf{r}; \xi) \quad \text{for all } \mathbf{r} \in \Omega. \tag{22}$$

We compute the gradient direction $\mathbf{grad}_{\tau_{in}} \mathcal{J}(\mathbf{r})$ using an adjoint scheme. We give here the main result (see the Appendix for details).

Theorem 1. *The gradient direction of $\mathcal{J}$ with respect to τ_{in} at each artificial time ξ is given by*

$$\mathbf{grad}_{\tau_{in}} \mathcal{J}(\mathbf{r}; \xi) = \int_0^T dt\, w \frac{h(v - v_{rest})^2 (v - 1)}{\tau_{in}^2} \tag{23}$$

where $h = h(\mathbf{r}, t)$ and $v = v(\mathbf{r}, t)$ are the solutions of our mathematical model using the distributions (17) and (18). In (23), T is the time interval over which the intracardiac recordings are taken, and $w = w(\mathbf{r}, t)$ solves the following adjoint equation

$$-\frac{\partial w}{\partial t} - \kappa \nabla^2 w + \left\{ h \frac{v(2 - 3v - v_{rest})}{\tau_{in}} - \frac{v_{rest}}{\tau_{out}} \right\} w = \frac{1}{4\pi} \sum_j \mathcal{R}_j \nabla^2 \frac{1}{|\mathbf{r} - \mathbf{r}_i|} \tag{24}$$

$$\mathbf{n} \cdot \nabla w(\mathbf{r}, t) = \frac{1}{4\pi} \sum_j \mathcal{R}_j \mathbf{n} \cdot \nabla \frac{1}{|\mathbf{r} - \mathbf{r}_i|} \quad \text{on } \partial\Omega \tag{25}$$

$$w(\mathbf{r}, T) = 0. \tag{26}$$

In these expressions, $\mathcal{R}_j \equiv \mathcal{R}_j(\psi(\xi)) = \phi_j(\psi(\xi)) - \tilde{\phi}_j$ denotes the mismatch between the measured data $\tilde{\phi}_j$ at each electrode site and the calculated one $\phi_j(\psi(\xi))$ using $\tau_{in}(\psi(\xi))$. Discretizing (20) by a straightforward finite difference time-discretization with time-step $\Delta\xi^{(n)} > 0$ in step n, and interpreting $\psi^{(n+1)} = \psi(\xi^{(n)} + \Delta\xi^{(n)})$ and $\psi^{(n)} = \psi(\xi^{(n)})$, we have the iteration

$$\psi^{(n+1)} = \psi^{(n)} + \Delta\xi^{(n)} f^{(n)}(\mathbf{r}), \qquad \psi^{(0)} = \psi_0. \tag{27}$$

To avoid the usual instabilities that arise from the use of the gradient direction computed directly from the adjoint formulation, we applied, previously to (27), a regularization strategy that smoothes the forcing terms $f^{(n)}(\mathbf{r})$. To this end, we convolve the unregularized gradient directions calculated by (23) with a Gaussian kernel of a given variance. Practically, this can be done by solving an initial value problem for the heat equation (for more details, see [28,43]. In Algorithm 1, we outline our algorithm to reconstruct the ischemic regions.

4. Numerical experiments

In the numerical experiments presented below, we consider a bi-dimensional cardiac tissue of size $\Omega = 2 \times 2$ cm^2 defined by the parameters shown in Table 1. Within the medium there might be one or several ischemic regions for testing the algorithm. Measurements were simulated with a second order finite difference Crank–Nicolson scheme for the spatial operators in a 100×100 grid. To discretize the resulting equations in time, we use a semi-implicit first order scheme where the nonlinear terms are treated explicitly. In all the experiments, we have added random fluctuations of 10% to the parameter values given in Table 1. The stimulation protocol consists on periodic pulses J_{stim} applied on a 0.8×0.8 mm^2 square at the upper-left corner boundary of the cardiac tissue. Each stimulation pulse has 2 ms length and 1 ms^{-1} amplitude. At the considered stimulation frequency (1.25 Hz) the steady state is reached after the second beat. For all experiments, the

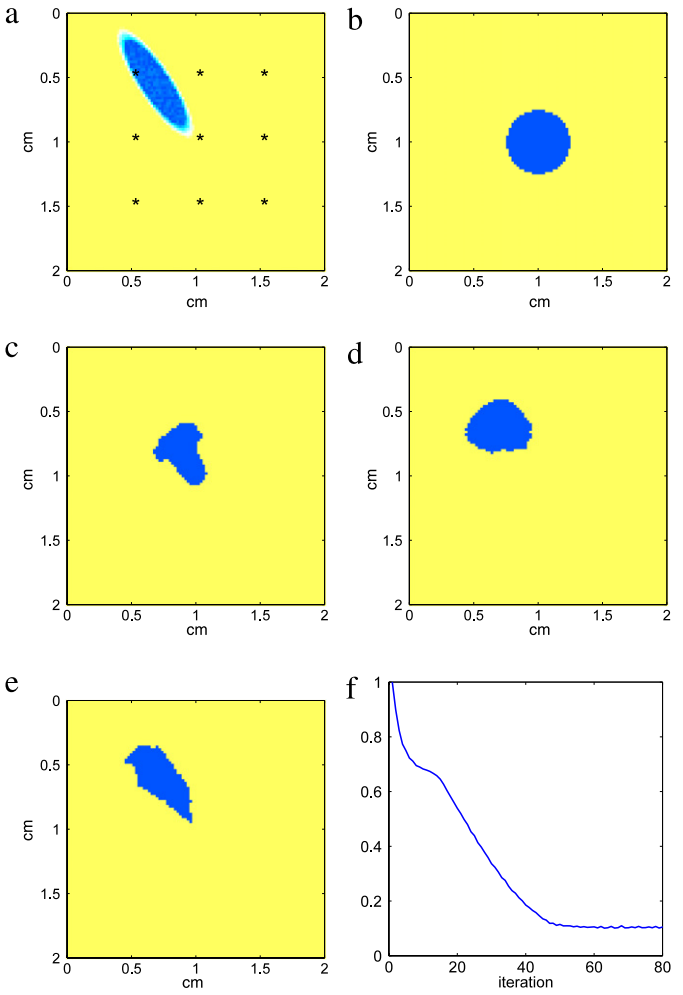

Fig. 4. First numerical experiment: reconstructing a single ischemia. (a) Reference τ_{in} profile. The (x, y) positions of the electrodes are shown with small stars. The electrodes are placed at $z = 0.5$ cm above the tissue. (b) Initial τ_{in} profile. (c), (d), (e) Reconstructed τ_{in} profiles at 15, 30 and 80 iterations, respectively. (f) Evolution of the cost during the reconstruction process (a.u.).

reconstruction algorithm is applied to a single cardiac cycle of length $T = 800$ ms in the steady state. In the first set of experiments, we reconstruct the shape of ischemia using measurements from 9 electrodes placed at 0.5 cm above the tissue. Fig. 4 illustrates the reconstruction process in the situation where a single ischemic region is located at the top left quadrant of the cardiac tissue. Panel (a) shows the (x, y) location of the electrodes along with the true τ_{in} profile which consists of a region with $\tau_{in} > 0.2$ ms surrounded by the healthy tissue with $\tau_{in} = 0.2$ ms. The reconstruction algorithm starts using an initial guess located at the center of the tissue (Fig. 4(b)). During the first iterations (Fig. 4(c) and (d)) the ischemic region moves toward its right location. Then, after 80 iterations stopping criterion is fulfilled, producing a final reconstruction as shown in Fig. 4(e). A comparison between the reconstructed and the real ischemic regions shows that the location, size and form have been reconstructed successfully. Fig. 4(e) represents the evolution of the cost functional (15). It is apparent that the cost functional (as well as the reconstructed shape) stabilizes after about 50 iterations. Fig. 5 shows the reconstruction process in the situation where two disconnected ischemic regions are considered under the same electrode configuration as the previous experiment. During the first iterations the reconstructed region breaks into two pieces (Fig. 5(b) and (c)) until the final estimation is achieved (Fig. 5(d)). As before, a comparison between the reconstructed and the real ischemia regions (depicted in Fig. 5(a) and (d), respectively) shows a very good estimate of the location, form and connectivity of the ischemia. Finally, in Fig. 6, we investigate the influence of the number of available measurements on the reconstruction results. Fig. 6(a) and (b) display the final reconstructions for the experiment shown in Fig. 4 when we use four and sixteen electrodes to carry out the inversion, respectively. Even with only four electrodes the algorithm is able to detect and locate the ischemia correctly. On the other hand, the shape of the reconstructed ischemic region is closer to the real one when we use sixteen electrodes. A similar behavior of the algorithm is observed in Fig. 6(c) and (d), which represents the same experiment as in Fig. 5 but using four and sixteen electrodes, respectively. With only four electrodes the reconstructions are satisfactory. However, the size and shape of the ischemic regions improve when more electrodes are used.

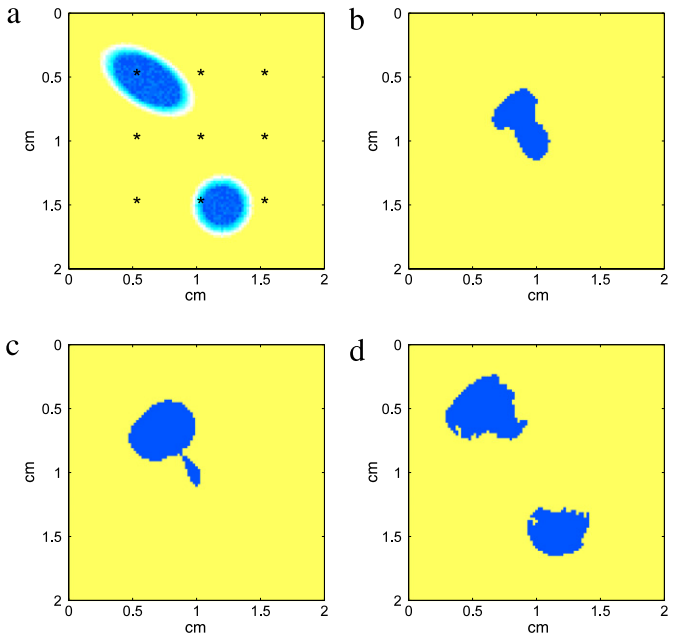

Fig. 5. Second numerical experiment: two non-connected ischemias. (a) reference τ_{in} profile. The (x, y) positions of the electrodes are shown with small stars. The electrodes are placed at $z = 0.5$ cm above the tissue. (b), (c) and (d) reconstructed τ_{in} profiles at 10, 30 and 80 iterations, respectively.

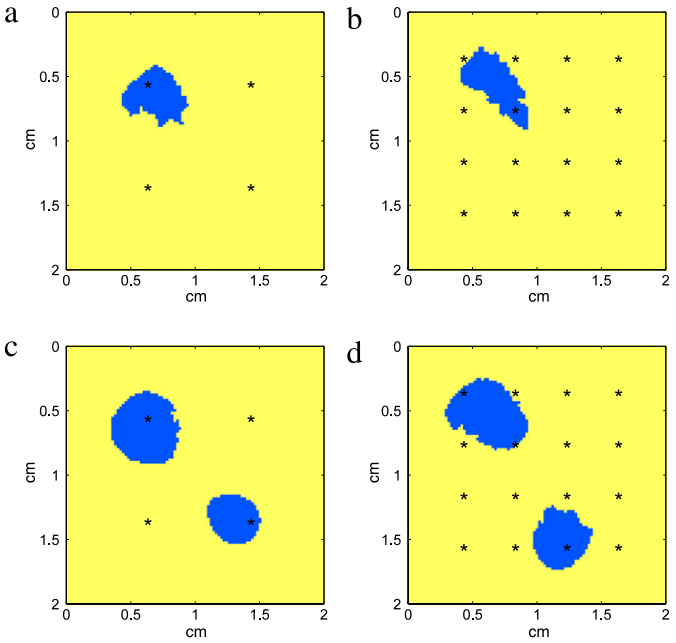

Fig. 6. Third numerical experiment: impact of the number of electrodes on the reconstructions. The (x, y) positions of the electrodes are shown with small stars. The electrodes are placed at $z = 0.5$ cm above the tissue. (a) and (b) are the final reconstructions using 4 and 16 electrodes, respectively (the reference τ_{in} profile is the same as in the first numerical experiment). (c) and (d) are the final reconstructions using 4 and 16 electrodes, respectively (the reference τ_{in} profile is the same as in the second numerical experiment).

5. Discussion and conclusions

Several approaches have been proposed in the literature to identify regions of ischemia from body surface potential measurements [44–47]. To carry out the inversion, these works usually consider a few hundreds of electrodes that record several time-independent frames during a cardiac cycle. Hence, the spatio-temporal correlations of the electrograms are not explicitly considered during the inversion. They also apply different techniques to this problem. In particular, Li and He estimated the size and position of myocardial infarction by minimizing the difference between simulated and measured

surface potentials over 200 electrodes using a machine learning algorithm [44]. Following a similar approach, Farina and Dössel proposed an optimization-based method over a space of 12 parameters which define the localization of infarction scars [45]. On the other hand, in [46,47] the authors use a level-set framework to identify ischemic regions which are characterized by a higher value of the resting potential. Thus, they only use information given at the resting phase of the cardiac cycle.

In this paper, we propose a different approach to reconstruct ischemic regions from a limited number of electrode recordings. Our approach relies on incorporating the knowledge of the cardiac excitation process into the level-set formulation. Hence, we incorporate the spatio-temporal correlation contained in the measurements through the cardiac propagation model. Furthermore, we propose appropriate variations of the model parameters to take into account the ischemia.

In the numerical experiments that we have presented in this paper, we considered a bi-dimensional model of the cardiac tissue. These numerical experiments are meant to serve as a proof of concept. Despite the lack of sophistication in them, we believe that our results show clearly that the proposed methodology may be very useful. However, future work has to be done in order to overcome limitations of the present study and to extend the performance of our method to more realistic scenarios. A detailed 3D model of the heart would have to be incorporated to demonstrate its potential. Nevertheless, we stress that the proposed methodology is neither limited to 2D geometries (in fact, level set techniques have been widely applied to 3D problems) nor to the specific two-current model used in this paper to describe the bioelectric propagation in the cardiac tissue. Any other cardiac model could be used as well without the interference in the rest of the algorithm.

Acknowledgments

The authors wish to thank Professor David Schaeffer for useful discussions and valuable comments during the preparation of this work.

This work was supported in part by FIS2010-18473, TEC2010-19263 and TSI-020100-2010469 Research Projects.

Appendix

We derive here Eq. (23). To compute a descent direction of the cost $\mathcal{J}$ (15) when τ_{in} varies subject to (6) and (7). To derive the adjoint equations, we build the Lagrange functional

$$\mathcal{L}(\tau_{in}; v(\mathbf{r}, t)) = \mathcal{J}(\tau_{in}) - \int_0^T \int_\Omega w \left\{ \frac{\partial v}{\partial t} - \kappa \nabla^2 v \right\} - \int_0^T \int_\Omega w \left\{ \frac{h(v - v_{rest})^2 (1 - v)}{\tau_{in}} \right\} + \int_0^T \int_\Omega w \left\{ \frac{v - v_{rest}}{\tau_{out}} \right\}. \tag{28}$$

Obviously, when v and h satisfy (5) $\mathcal{L} = \mathcal{J}$ for all w. Hence, we have incorporated Eq. (5) into the function $\mathcal{L}$. We now take the variation of (28):

$$\delta \mathcal{L} = \frac{\partial \mathcal{L}}{\partial \tau_{in}} \delta \tau_{in} - \frac{\partial \mathcal{L}}{\partial v} \delta v. \tag{29}$$

Note that if the last term is zero then $\delta \mathcal{L} = \delta \mathcal{J}$. Since, so far, w is an arbitrary function, we can choose it so this last term vanishes. Hence, we impose that

$$\frac{\partial \mathcal{L}}{\partial v} \delta v = 0. \tag{30}$$

From this condition, we derive the adjoint equation. To first order, we can write

$$\frac{\partial \mathcal{L}}{\partial v} \delta v = \mathcal{L}(\tau_{in}, v + \delta v) - \mathcal{L}(\tau_{in}, v) = \frac{\partial \mathcal{J}}{\partial v} \delta v - \int_0^T \int_\Omega v \left\{ \frac{\partial \delta v}{\partial t} - \kappa \nabla^2 \delta v + \frac{h v (2 - 3v - v_{rest})}{\tau_{in}} \delta v - \frac{v_{rest}}{\tau_{out}} \delta v \right\}. \tag{31}$$

Integrating by parts, applying the divergence theorem, and using (6) and (7) we obtain

$$\frac{\partial \mathcal{L}}{\partial v} \delta v = \frac{1}{4\pi} \int_0^T \sum_j \mathcal{R}_j \left\{ \int_\Omega \delta v \kappa \nabla^2 \frac{1}{|\mathbf{r} - \mathbf{r}_j|} - \int_{\partial \Omega} \delta v \mathbf{n} \cdot \kappa \nabla \frac{1}{|\mathbf{r} - \mathbf{r}_i|} \right\} - \int_0^T \int_\Omega \delta v \left\{ -\frac{\partial w}{\partial t} - \kappa \nabla^2 w + \left\{ \frac{h v (2 - 3v - v_{rest})}{\tau_{in}} - \frac{v_{rest}}{\tau_{out}} w \right\} \right\} \tag{32}$$

where we have imposed that $w(\mathbf{r}, t = T) = 0$. Since $\frac{\partial \mathcal{L}}{\partial v}\delta v$ is zero for all δv, we rearrange the terms on the right hand side and we identify (32) as the weak formulation of the problem defined by Eqs. (24)–(25). The minus sign in front of the time derivative in (24) means backward time integration. Therefore, if we select w so that it satisfies the adjoint problem (24)–(25) we have that

$$\delta \mathcal{J} = \delta \mathcal{L} = \frac{\partial \mathcal{L}}{\partial \tau_{in}} \delta \tau_{in} = \langle \mathbf{grad}_{\tau_{in}} \mathcal{L}, \delta \tau_{in} \rangle_P, \tag{33}$$

from where

$$\delta \mathcal{J} = \langle \mathbf{grad}_{\tau_{in}} \mathcal{J}, \delta \tau_{in} \rangle_P = \int_\Omega d\mathbf{r} \int_0^T dt\, w \frac{h(v - v_{rest})^2 (v - 1)}{\tau_{in}^2} \delta \tau_{in}. \tag{34}$$

To obtain (34), we have taken the derivative of (28) with respect to τ_{in}. Finally, we identify

$$\mathbf{grad}_{\tau_{in}} \mathcal{J}(\mathbf{r}) = \int_0^T dt\, w \frac{h(v - v_{rest})^2 (v - 1)}{\tau_{in}^2}. \tag{35}$$

With this we have proven Eq. (23).

References

[1] A.J. Pullan, L.K. Cheng, M. Buist, Mathematically Modelling the Electrical Activity of the Heart: From Cell to Body Surface and Back Again, World Scientific Publishing, 2005.
[2] F.B. Sachse, Computational Cardiology: Modeling of Anatomy, Electrophysiology, and Mechanics, Springer-Verlag, New York Inc., 2004.
[3] R. Clayton, O. Bernus, E. Cherry, H. Dierckx, F. Fenton, L. Mirabella, et al., Models of cardiac tissue electrophysiology: progress, challenges and open questions, Prog. Biophys. Mol. Biol. 104 (2011) 22–48.
[4] Y. Rudy, B.J. Messinger-Rapport, The inverse problem in electrocardiography: solutions in terms of epicardial potentials, Crit. Rev. Biomed. Eng. 16 (3) (1988) 215–268.
[5] R.S. MacLeod, D.H. Brooks, Recent progress in inverse problems in electrocardiology, IEEE Eng. Med. Biol. Mag. 17 (1) (1998) 73–83.
[6] R.J. Schilling, N.S. Peters, D.W. Davies, Simultaneous endocardial mapping in the human left ventricle using a noncontact catheter: comparison of contact and reconstructed electrograms during sinus rhythm, Circulation 98 (9) (1998) 887–898.
[7] E.J. Voth, The inverse problem of electrocardiography: industrial solutions and simulations, Int. J. Bioelectromagnetism 7 (2) (2005) 191–194.
[8] R.M. Gulrajani, The forward and inverse problems of electrocardiography, IEEE Eng. Med. Biol. Mag. 17 (5) (1998) 84–101.
[9] B.J. Messinger-Rapport, Y. Rudy, Computational issues of importance to the inverse recovery of epicardial potentials in a realistic heart-torso geometry, Math. Biosci. 97 (1) (1989) 85–120.
[10] Y. Rudy, H.S. Oster, The electrocardiographic inverse problem, Crit. Rev. Biomed. Eng. 20 (1–2) (1992) 25–45.
[11] H.S. Oster, Y. Rudy, The use of temporal information in the regularization of the inverse problem of electrocardiography, IEEE Trans. Biomed. Eng. 39 (1) (1992) 65–75.
[12] F. Greensite, G. Huiskamp, An improved method for estimating epicardial potentials from the body surface, IEEE Trans. Biomed. Eng. 45 (1) (1998) 98–104.
[13] D.H. Brooks, G.F. Ahmad, R.S. MacLeod, G.M. Maratos, Inverse electrocardiography by simultaneous imposition of multiple constraints, IEEE Trans. Biomed. Eng. 46 (1) (1999) 3–18.
[14] K. Berrier, D. Sorensen, D. Khoury, Solving the inverse problem of electrocardiography using a duncan and horn formulation of the kalman filter, IEEE Trans. Biomed. Eng. 51 (3) (2004) 507–515.
[15] G. Huiskamp, F. Greensite, A new method for myocardial activation imaging, IEEE Trans. Biomed. Eng. 44 (6) (1997) 433–446.
[16] G. Huiskamp, A. Van Oosterom, The depolarization sequence of the human heart surface computed from measured body surface potentials, IEEE Trans. Biomed. Eng. 35 (12) (1988) 1047–1058.
[17] B. Tilg, G. Fischer, R. Modre, F. Hanser, B. Messnarz, M. Schocke, et al., Model-based imaging of cardiac electrical excitation in humans, IEEE Trans. Med. Imaging 21 (9) (2002) 1031–1039.
[18] B. Messnarz, B. Tilg, R. Modre, G. Fischer, F. Hanser, A new spatiotemporal regularization approach for reconstruction of cardiac transmembrane potential patterns, IEEE Trans. Biomed. Eng. 51 (2) (2004) 273–281.
[19] A. Ghodrati, D.H. Brooks, G. Tadmor, R.S. MacLeod, Wavefront-based models for inverse electrocardiography, IEEE Trans. Biomed. Eng. 53 (9) (2006) 1821–1831.
[20] Y. Serinagaolu, D.H. Brooks, R.S. MacLeod, Improved performance of bayesian solutions for inverse electrocardiography using multiple information sources, IEEE Trans. Biomed. Eng. 7 (10) (2006) 2024–2034.
[21] B. Yilmaz, R.S. MacLeod, B.B. Punske, B. Taccardi, D.H. Brooks, Venous catheter based mapping of ectopic epicardial activation: training data set selection for statistical estimation, IEEE Trans. Biomed. Eng. 52 (11) (2005) 1823–1831.
[22] S. Ghosh, Y. Rudy, Application of l1-norm regularization to epicardial potential solution of the inverse electrocardiography problem, Ann. Biomed. Eng. 37 (5) (2009) 902–912.
[23] S. Osher, J. Sethian, Fronts propagating with curvature-dependent speed: algorithms based on Hamilton Jacobi formulations, J. Comput. Phys. 79 (1988) 12–49.
[24] F. Santosa, A level set approach for inverse problems involving obstacles, ESAIM Control Optim. Calc. Var. 1 (1996) 17–33.
[25] O. Dorn, E. Miller, C. Rappaport, A shape reconstruction method for electromagnetic tomography using adjoint fields and level sets, Inverse Problems 16 (2000) 1119–1156.
[26] D. Álvarez, P. Medina, M. Moscoso, Fluorescence lifetime imaging from time resolver measurements using a shape-based approach, Opt. Express 17 (11) (2009) 8843–8855.
[27] N. Irishina, O. Dorn, M. Moscoso, Microwave imaging for early breast cancer detection using a shape-based strategy, IEEE Trans. Biomed. Eng. 56 (4) (2009) 1143–1153.
[28] O. Dorn, D. Lesselier, Level set methods for inverse scattering, Inverse Problems 22 (2006) R67–R131.
[29] B.F. Nielsen, M. Lysaker, A. Tveito, On the use of the resting potential and level set methods for identifying ischemic heart disease: an inverse problem, J. Comput. Phys. 220 (2007) 771–790.
[30] C.C. Mitchell, D.G. Schaeffer, A two-current model for the dynamics of cardiac membrane, Bull. Math. Biol. 65 (5) (2003) 767–793.
[31] J.W. Cain, D.G. Schaeffer, Shortening of cardiac action potential duration near an insulating boundary, Math. Med. Biol. 25 (1) (2008) 21–36.
[32] D. Schaeffer, W. Ying, X. Zhao, Asymptotic approximation of an ionic model for cardiac restitution, Nonlinear Dynam. 51 (1–2) (2008) 189–198.

[33] M. Beck, C.K.R.T. Jones, D. Schaeffer, M. Wechselberger, Electrical waves in a one-dimensional model of cardiac tissue, SIAM J. Appl. Dyn. Syst. 7 (4) (2008) 1558–1581.
[34] C.S. Henriquez, A.A. Papazoglou, Using computers models to understand the roles of tissue structure and membrane dynamics in arrhythmogenesis, Proc. IEEE 84 (1996) 334–354.
[35] H. Morena, M.J. Janse, J.W. Fiolet, W.J. Krieger, H. Crijns, D. Durrer, Comparison of the effects of regional ischemia, hypoxia, hyperkalemia, and acidosis on intracellular and extracellular potentials and metabolism in the isolated porcine heart, Circ. Res. 46 (5) (1980) 634–646.
[36] I. Kodama, A. Wilde, M.J. Janse, D. Durrer, K. Yamada, Combined effects of hypoxia, hyperkalemia and acidosis on membrane action potential and excitability of guinea-pig ventricular muscle, J. Mol. Cell. Cardiol. 16 (3) (1984) 247–259.
[37] R.M. Shaw, Y. Rudy, Electrophysiologic effects of acute myocardial ischemia. a mechanistic investigation of action potential conduction and conduction failure, Circ. Res. 80 (1) (1997) 124–138.
[38] A. Cimponeriu, C.F. Starmer, A. Bezerianos, A theoretical analysis of acute ischemia and infarction using ecg reconstruction on a 2-d model of myocardium, IEEE Trans. Biomed. Eng. 48 (1) (2001) 41–54.
[39] J. Ferrero, B. Trénor, B. Rodríguez, J. Saiz, Electrical activity and reentry during acute regional myocardial ischemia: insights from simulations, Int. J. Bifurcation Chaos 13 (12) (2003) 3703–3715.
[40] B. Trenor, L. Romero, J.M.J. Ferrero, J. Saiz, G. Molto, J.M. Alonso, Vulnerability to reentry in a regionally ischemic tissue: a simulation study, Ann. Biomed. Eng. 35 (10) (2007) 1756–1770.
[41] J. Malmivuo, R. Plonsey, Bioelectromagnetism—Principles and Applications of Bioelectric and Biomagnetic Fields, Oxford University Press, New York, 1995.
[42] K. Gima, Y. Rudy, Ionic current basis of electrocardiographic waveforms: a model study, Circ. Res. 90 (2002) 889–896.
[43] D. Álvarez, O. Dorn, N. Irishina, M. Moscoso, Crack reconstruction using a level-set strategy, J. Comput. Phys. 228 (2009) 5710–5721.
[44] G. Li, B. He, Non-invasive estimation of myocardial infarction by means of a heart-model-based imaging approach: a simulation study, Med. Biol. Eng. Comput. 42 (1) (2004) 128–136.
[45] D. Farina, O. Dossel, Model-based approach to the localization of infarction, Comput. Cardiol. 2007 (2007) 173–176.
[46] M.C. MacLachlan, B.F. Nielsen, M. Lysaker, A. Tveito, Computing the size and location of myocardial ischemia using measurements of st-segment shift, IEEE Trans. Biomed. Eng. 53 (6) (2006) 1024–1031.
[47] T.S. Ruud, B.F. Nielsen, M. Lysaker, J. Sundnes, A computationally efficient method for determining the size and location of myocardial ischemia, IEEE Trans. Biomed. Eng. 56 (2) (2009) 263–272.